Materials Horizons

ROYAL SOCIETY OF CHEMISTRY

REVIEW

View Article Online
View Journal | View Issue

Cite this: *Mater. Horiz.*, 2025, **12**, 6124

The emergence of metal-free molecular perovskites: challenges and opportunities

Loreta A. Muscarella, *[a] Gianluca Bravetti [b] and Jovana V. Milić *[bc]

Received 22nd December 2024,
Accepted 11th April 2025

DOI: 10.1039/d4mh01877j

rsc.li/materials-horizons

Perovskite materials are increasingly important in a variety of optoelectronic applications. Some of these functional materials also exhibit ferroelectric properties, making them promising in memory elements, sensors, and energy technologies. While they exhibit extraordinary performances, their instabilities often hinder practical applications and toxic metal components cause environmental concerns. In the last few years, metal-free molecular perovskites (MOPs) have emerged, featuring ferroelectric properties that outperform conventional perovskite ferroelectrics while offering an environmentally friendly and cost-effective alternative relevant to optoelectronics. We review the structural and optoelectronic characteristics of this new class of materials, as well as preparation techniques, with challenges and opportunities for future applications.

Wider impact

Perovskites have become one of the leading semiconductors in modern optoelectronics. These materials are based on the ABX_3 composition, defined by the corner-sharing $\{MX_6\}$ octahedral framework comprising divalent metal (B) cations and, most commonly, oxide or halide (X) anions while hosting central A cations within their cavity. They feature unique optoelectronic characteristics, as well as ferroelectric properties, which are relevant to energy technologies, sensing, and memory elements. However, they are composed of toxic metal components, such as lead, which cause environmental concerns, posing a requirement for alternative and more sustainable solutions. Over the last few years, metal-free perovskite alternatives based on all-organic molecular framework materials have emerged. Their corresponding ABX_3 perovskite structure is composed of ammonium (NH_4^+) B cations and divalent (A^{2+}) organic cations, featuring ferroelectric characteristics that outperform conventional perovskite ferroelectrics while offering a more environmentally friendly alternative. These organic materials promise to advance optoelectronics toward more sustainable technologies, yet their synthetic accessibility and material scope remain limited, stimulating investigations and developments toward their fundamental understanding and innovative applications. This review discusses the challenges associated with the emerging metal-free perovskite materials while outlining opportunities for their development and applications.

Introduction

Perovskite materials have become one of the leading candidates in modern optoelectronics, from photovoltaics to light-emitting diodes and detectors.[1] They are versatile materials based on typical ABX_3 perovskite structures that are primarily oxides (X = O) or halides (X = I, Br, and Cl) (Fig. 1, left). Some of these systems have attracted attention due to their ferroelectric properties,[2,3] which involve spontaneous polarisation that can be reversed by applying an external electric field, important in low-power non-volatile memory, sensors, and energy harvesting.[4–6] This mostly involved ferroelectric ceramic and perovskite oxide materials, such as $Pb(Zr_xTi_{1-x})O_3$ and $BaTiO_3$.[5,6] However, these conventional ferroelectrics face limitations regarding scalability, cost-effectiveness, and environmentally friendly processing.[5,6] In addition, most perovskite and ferroelectric materials are based on toxic metal components and are sensitive to temperature variations, humidity, and mechanical stress; thus, reducing the metal content while improving their overall stability is essential for long-term reliability.[5] Overcoming the challenges associated with processing, stability, and integration of perovskite ferroelectrics would help unlock their full potential for more efficient and sustainable technologies. This has stimulated the development of organic ferroelectrics, which are more environmentally friendly and easily processable materials compatible with integration into flexible technologies.[4] However, they exhibit lower performance metrics than inorganic systems,[2] posing an ongoing strive to develop competitive organic materials.

Metal-free molecular perovskites (MOPs) have recently emerged as promising alternative ferroelectric materials.[7–10]

[a] *Vrije Universiteit Amsterdam, De Boelelaan 1105, Amsterdam, 1081 HV, The Netherlands. E-mail: l.a.muscarella@vu.nl*
[b] *Adolphe Merkle Institute, University of Fribourg, Chemin des Verdiers 4, Fribourg, 1700, Switzerland. E-mail: jovana.milic@unifr.ch*
[c] *University of Turku, Department of Chemistry, Henrikinkatu 2, Aurum, Turku, 20500, Finland. E-mail: jovana.milic@utu.fi*

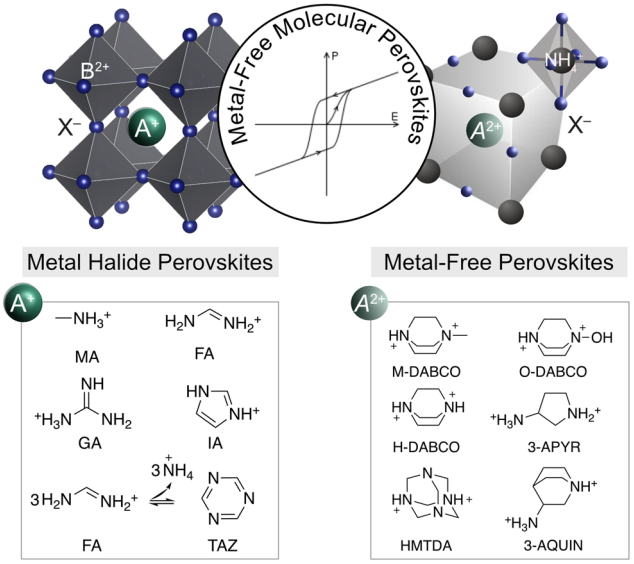

Fig. 1 Perovskite structural representation. Schematic of the structure of metal halide perovskites (left) and metal-free molecular perovskites (MOPs; right) with characteristic A^+ and A^{2+} cations. MA = methylammonium; FA = formamidinium; GA = guanidinium; IA = imidazolium; TAZ = triazine, a product of FA-based perovskite reactivity; H-DABCO = *N*,*N*-diazabicyclo[2,2,2]octonium; M-methyl, O – hydroxyl; HTMDA = hexamethylenetetrammonium; 3-APYR = 3-ammoniopyrrolidinium; 3-AQUIN = 3-ammonioquinuclidinium. Other examples are piperazinium (PAZE) and homopiperazinium (HPIP), Fig. 2.

Unlike conventional perovskite ferroelectrics, these metal-free systems do not pose environmental concerns associated with toxic metal components, such as lead, and they could be fabricated from aqueous solutions, showing desirable mechanical[11] and potential optoelectronic characteristics.[12,13] While ferroelectric behaviour is under debate for three-dimensional metal halide perovskites[14] and disputed in some of the two-dimensional halide perovskites, including hybrid and double perovskites,[15–19] MOPs show the capacity to outperform conventional perovskite ferroelectrics and find applications in modern flexible (opto)electronics.[7,8]

Here, we review this emerging class of metal-free molecular perovskites from the perspective of their unique structural characteristics and discuss challenges associated with their processing, focusing on halide perovskite compositions. Finally, we consider opportunities for their development and applications.

Metal-free molecular perovskites

Material scope

MOPs are defined by the ABX_3 perovskite structures (Fig. 1, right)[3] based on a central protonated A-cation (A^{2+}) within an $\{(NH_4)X_6\}$-based octahedral corner-sharing framework defined by the B site ammonium $(NH_4)^+$ and the X-site anion.[7] Their X-site can be either a halide (I^-, Br^-, and Cl^-) or a pseudo-halide anion (*e.g.*, $HCOO^-$, BF_4^-, and ClO_4^-), whereas the central organic (A) cation can be *N*,*N*-diazabicyclo[2,2,2]octonium (H-DABCO) and its derivatives (O-DABCO or M-DABCO), piperazine (PAZE), hexamethylenetetramine (HTMA), 3-ammonioquinuclidinium (3-AQUIN) or 3-ammoniopyrrolidinium (3-APYR; Fig. 1, right).[7,20,21] The overall structure is held together by hydrogen bonding interactions, stabilising the 3D framework.[7] The first MOP was reported in 2002,[21] sparking ongoing research into their optoelectronic and ferroelectric properties, which has notably accelerated over the past five years (Fig. 2),[7–10] driven by advancements in the understanding of their ferroelectric, mechanical, and optoelectronic characteristics[7–13,20–26] and their relevance to next-generation technologies. The first example was based on piperazinium (PAZE) central cations and their ammonium chloride hydrates of the $(PAZE)NH_4Cl_3 \times 2H_2O$ composition, with a 3D perovskite corner-sharing $\{NH_4Cl_6\}$-based octahedral framework enclosed by two water molecules in an ABX_3C structure (Fig. 2a).[21] This has set the basis for other ammonium-halide-based ABX_3 perovskite frameworks incorporating DABCO-based cations (Fig. 2b).[8] The A sites relied on (OH or methyl, M; Fig. 2c) DABCO, chiral 3-AQUIN and 3-APYR, HMTA, and PAZE.

In addition to the 3D systems, early examples also involved a low-dimensional (1D) face-sharing octahedral framework incorporating DABCO ammonium chloride of ANH_4Cl_3 composition (Fig. 2b).[21] Recently, the first 2D system was reported incorporating homopiperazinium (HPIP) in the $(HPIP)_2(NH_4)I_5$ composition (Fig. 2d), with a related 1D $(HPIP)_3(NH_4)I_7$ analogue, as single crystals are used to showcase the capacity to access low-dimensional structures of MOPs through compositional engineering.[25] While B-site cations play an essential role in dimensionality control, the anisotropy and geometric compatibility of A cations are critical, opening the way for other low-dimensional structures. Their versatility and structure–property relationships remain unexploited and require appropriate synthesis methods.

Materials synthesis

MOPs have primarily been studied in the form of single crystals grown from aqueous solutions.[7,8,11] They provide an ideal platform for fundamental studies due to their low-defect nature, which allows for precise characterisation of structural, optical, and electronic properties. The absence of grain boundaries and minimal defects eliminates extrinsic factors that could obscure intrinsic material behaviours, such as charge carrier dynamics and ferroelectric properties.[5,12,13] The most prevalent method for growing single crystals is the slow evaporation. This process involves dissolving organic cations and ammonium halides in suitable solvents—typically acidic water media or alcohols—and allowing the solvent to evaporate slowly under controlled conditions.[7,8] For instance, single crystals of $(H\text{-}DABCO)(NH_4)Br_3$ were synthesised by dissolving equimolar amounts of DABCO and HBr in deionised water to form the organic cation solution, followed by adding ammonium bromide.[12] Over several days, slow evaporation of the solvent led to the formation of high-quality single crystals suitable for electrical measurements and structural analysis. The careful control of the solvent evaporation rate was crucial

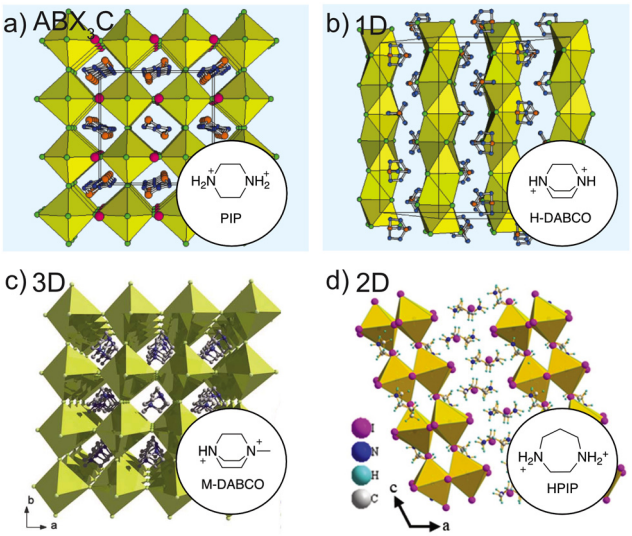

Fig. 2 Representative MOP structures. (a) 3D (PAZE)NH_4Cl_3 × $2H_2O$. The view down [100] orientation showing the perovskite octahedral network encapsulating piperazinium (PAZE) and water molecules. (b) 1D (H-DABCO)NH_4Cl_3, viewed down [210] orientation, showing the face-sharing {NH_4Cl_6} octahedra propagating along [001], interspersed by stacks of H-DABCO cations. Reproduced with permission from ref. 21. Copyright 2002 American Chemical Society. (c) Packing diagram of (M-DABCO)NH_4I_3 at 293 K. Reproduced with permission from ref. 8. Copyright 2018 Science. H atoms are omitted for clarity; {NH_4X_6} octahedra are shown in yellow, Cl atoms in green, N in orange, C in blue or grey, and O in pink. (d) 2D $(HPIP)_2NH_4I_5$ perovskite. Reproduced with permission from ref. 25. Copyright 2024 John Wiley and Sons.

to minimise the formation of defects and ensure the growth of well-ordered crystals. Key parameters such as solvent, concentration, and temperature are crucial for successful crystal growth.[12,26] The solvent must adequately dissolve the reactants while promoting slow crystallisation and maintaining a supersaturated solution to facilitate nucleation without rapid precipitation. Temperature fluctuations can affect solubility and evaporation rates, so a constant temperature is often employed to ensure consistent growth conditions. Another widely used method has been slow cooling,[8,12] where a hot saturated solution of the precursors is gradually cooled to room temperature. It was shown that using this method allowed the growth of single crystals of MOPs such as (M-DABCO)$(NH_4)I_3$.[8] A hot saturated solution of the organic cation and ammonium iodide in water (80 °C) was slowly cooled to room temperature over several hours. As the temperature decreases, the solubility of the solutes diminishes, leading to supersaturation and subsequent crystal growth. This offers the advantage of controlled nucleation, allowing existing crystals to grow larger, thus minimising thermal stress and defects within the perovskite lattice.[27]

Despite the utility of these solution-based methods, they present several challenges. The solubility limitations of certain organic cations, particularly those with aromatic structures, restrict the range of materials that can be accessed. Moreover, the slow growth rates and meticulous control required are incompatible with large-scale production, limiting the practicality of these methods. Finally, material waste due to solvent evaporation and crystallisation inefficiency contributes to costs and environmental concerns. To overcome these limitations of solution-based synthesis, mechanosynthesis has emerged as a promising alternative.[28] This solvent-free method involves inducing chemical reactions through mechanical force, typically by grinding.[28,29] Mechanosynthesis addresses environmental concerns by eliminating the need for solvents and circumvents solubility limitations associated with traditional synthesis.[30,31] In the case of MOPs, it could provide alternatives to poorly soluble organic cations, which are challenging to produce *via* solution methods.[29,32] The method is also scalable and efficient, allowing for better control in specific optoelectronic applications.[28,33–38] These strategies remain underexploited in MOP materials and devices.[28]

In addition, expanding the compositional diversity of MOPs is relevant. Novel organic cations with tailored properties can lead to perovskites with customised optoelectronic characteristics. To this end, computational studies[10] can guide the selection of promising candidates by predicting structural and electronic properties. Exploring alternative anions beyond halides, like pseudohalides,[39,40] may also provide access to materials with unique characteristics. Moreover, integrating other materials, such as conductive polymers or graphene, could enhance properties and open new application areas. Combining perovskites into multilayer device architectures may improve performance in applications like photovoltaics and photodetectors, where environmental stability remains a crucial limitation for practical applications. Understanding degradation mechanisms under various environmental conditions will inform strategies to enhance robustness.

Overall, accessing MOPs *via* different synthesis methods, including single-crystal growth, solution-based techniques, and mechanosynthesis, is crucial for their better understanding and expanding their applicability. While traditional methods remain invaluable for fundamental studies, mechanosynthesis could offer a scalable, environmentally friendly route to produce materials suitable for practical applications, which should be further explored. By overcoming the challenges related to reproducibility, purity, and integration, new synthetic methods pave the way for advanced perovskite materials with tailored properties. This progress can not only expand the compositional space but also facilitate the incorporation into next-generation optoelectronic devices, contributing to the advancement of sustainable and efficient next-generation technologies.

Material characteristics and applications

Optoelectronic properties

The synthetic challenges associated with MOPs have limited the investigation of their optoelectronic properties, with most research being theoretical or centered on single crystals.[7,10,12,32,33,41] The key optoelectronic properties, such as optical absorption, photoluminescence (PL), photoconductivity,

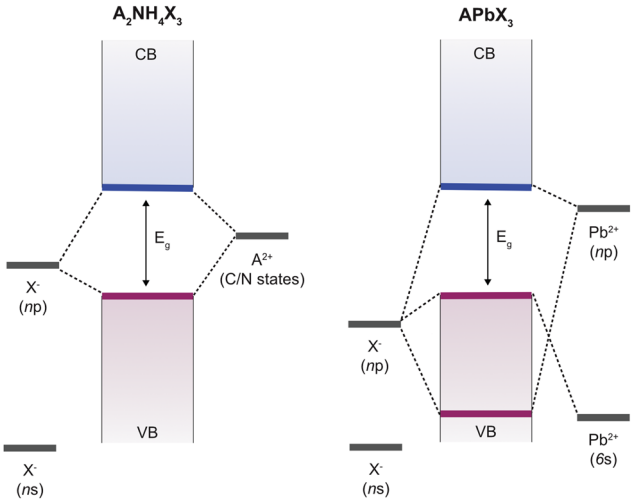

Fig. 3 Optoelectronic propertes of MOPs. Schematic representation of the orbital model with the VB and CB in MOPs (left) and more traditionally used lead-based hybrid perovskites (right) in optoelectronics.

carrier mobility and lifetime, trap states, defect density, and quantum efficiency, are essential in determining applications.

For photovoltaic applications, long charge carrier lifetimes and extended diffusion lengths are crucial, as they allow carriers to travel further to the electrodes before recombining, directly enhancing the power conversion efficiency. Similarly, low trap densities reduce energy losses and improve charge collection, contributing to overall device performance. In light-emitting diodes (LEDs), efficient charge transport and reduced trap states are critical for minimising non-radiative recombination, which leads to energy losses. Long carrier lifetimes and high mobility ensure that more carriers recombine radiatively, improving the overall light-emission efficiency and brightness. For photodetectors, long carrier lifetimes and efficient charge transport are essential for high sensitivity and fast response times, allowing the detection of low light with reduced noise.

Optoelectronic properties are intrinsically linked to the electronic structure and the corresponding valence (VB) and conduction (CB) bands, defining the bandgap and dictating the interaction with light (Fig. 3). The organic components influence band alignment, exciton binding energies, and charge carrier dynamics, making them distinct from conventional inorganic or hybrid materials. In lead-halide perovskites, as the most commonly used halide perovskite semiconductors, the VB maximum is formed by an antibonding combination of halogen np orbitals (Cl-3p, Br-4p or I-5p) and Pb s orbitals (Pb-6s), and the CB minimum by an antibonding combination of Pb p orbitals (Pb-6p) with negligible coupling with that of halogen np orbitals.[42,43] In contrast, density functional theory (DFT) calculations[7,8,10,41] show that the majority of MOPs features the VBM primarily composed by the interaction of halogen p orbitals, while the CBM is mainly defined by hybrid orbitals (carbon and nitrogen) of A-type cations, suggesting that tuning the bandgaps of this family of perovskites depends strongly on the modification of the A-type organic cation and halide ions (Fig. 3). These computed band characteristics also suggest that there is no strong bonding but only electrostatic interactions between A^{2+} cations and the halogens, with the exception of piperazinium, in which case the CBM is formed by a combination of the A cations and halogen *s* orbitals.[32,44] Overall, the CB in MOPs differs significantly from that of lead halide perovskites, making it an inappropriate benchmark, where the A cation has no direct impact on the bandgap transition, as it does not play a role in the formation of the VB and CB. Instead, the optoelectronic properties compare closer to the molecular systems defining the halide perovskite framework.

Due to these unique structural features and frontier band characteristics,[10] a method for estimating the bandgaps of MOPs was proposed by calculating the energies of the lowest unoccupied molecular orbital (LUMO) of the A cations. The presence of a strong electron-withdrawing group lowers the LUMO energy of the organic cation, and therefore the CB minimum, leading to an estimated reduction of the bandgap.[10] While this method can predict the general trend of bandgap in MOPs as a function of the divalent A cation, experimental measurements often reveal discrepancies. For example, the absorption and PL spectra of (M-DABCO)NH_4I_3 crystals revealed an indirect bandgap energy (E_g) of 4.95 eV,[45] whereas theoretical predictions suggested that E_g is around 4 eV,[10] implying additional factors influencing electronic properties.

In contrast, replacing halides is predicted to result in a gradual shift in the band nature from indirect to direct, accompanied by a reduction in bandgap values from 5.89 eV (indirect) to 5.25 eV (direct) and 4.71 eV (direct) for Cl-, Br- and I-based materials, respectively.[10] When pseudohalides as PF_6^- are used, the material exhibits a larger band value of 7.13 eV.[46] So far, only iodide-based (M-DABCO)NH_4I_3 exhibits PL under ultraviolet excitation.[8,45,47] First-principles calculations[10,47–48] suggest that halogen vacancies could be the source of low-energy optical absorption and PL of MOPs. This would suggest that PL can be related to an optically active center rather than a band-to-band transition.[49] Instead, self-trapped excitons (STEs) were proposed as the origin of the luminescence of the MOP crystals.[45] The PL quantum yield (PLQY) of (M-DABCO)$(NH_4)I_3$ was measured to be as high as 50%,[45] higher than the highest values reported for Pb-free perovskite crystals ($Cs_4MnBi_2Cl_{12}$: 25.7% and $Cs_2InBr_5{\cdot}H_2O$: 33%).[50,51] The charge carrier type and mobility, carrier lifetime, diffusion length, and trap density directly influence the efficiency of charge transport, recombination processes, and light emission.

MOPs exhibit a wide range of carrier lifetime–mobility ($\mu\tau$) product and trap density (N_t) values, depending on their composition and structure. For example, crystals of (H-DABCO)NH_4Br_3 demonstrated p-type conductivity with charge carrier lifetimes around 0.5 ms and diffusion lengths in the order of tens of micrometers. Their $\mu\tau$ product is on the order of 10^{-3} cm^2 V^{-1} for holes and 10^{-4} cm^{-2} V^{-1} for electrons, with trap densities ranging from 10^{10} to 10^{11} cm^{-3},[12] comparable to lead-halide perovskites. Similarly, (M-DABCO)$(NH_4)I_3$ crystals

Table 1 Reported carrier lifetime–mobility ($\mu\tau$) product and trap densities (N_t) for various MOP compositions as single crystals (SC) or thin films

Composition	$\mu\tau$ ($cm^2\ V^{-1}$)	N_t (cm^{-3})	Type	Ref.
(H-DABCO)NH_4Br_3	1.2×10^{-3} (holes) 3.1×10^{-4} (electrons)	10^{10} and 10^{11} cm^{-3}	SC	12
(M-DABCO)NH_4I_3	6.7×10^{-4}	5.65×10^{9}	SC	45
(M-DABCO)$NH_4(PF_6)$	1.56×10^{-4}	1.03×10^{10}	SC	46
(PAZE)$NH_4I_3{\cdot}H_2O$	1.30×10^{-6}	2.21×10^{15}	Films	44
(PAZE)$NH_4Br_3{\cdot}H_2O$	1.08×10^{-6}	1.71×10^{14}	Films	44
(PAZE)$NH_4Cl_3{\cdot}H_2O$	1.19×10^{-6}	1.91×10^{14}	Films	44
(N-DABCO)NH_4Br_3	3.05×10^{-4}	4.69×10^{9}	SC	56

exhibit $\mu\tau$ values in the range of 10^{-4} to 10^{-3} $cm^2\ V^{-1}$, with trap densities around 10^9 cm^{-3},[45,47] which are lower than those observed in the lead-based counterparts.[52,53] In systems where PF_6^- pseudohalides replace the halide, such as (M-DABCO)$(NH_4)(PF_6)_3$, the $\mu\tau$ product remains comparable to iodide-based analogues, but the trap density increases by an order of magnitude.[46] (PAZE)$NH_4Cl_3 \times 2H_2O$-based films exhibit lower $\mu\tau$ values, around 10^{-6} $cm^2\ V^{-1}$, with trap densities ranging from 10^{14} to 10^{15} cm^{-3},[47] similar to silicon[54] and CdTe.[55] Similarly, aminoazanium-based perovskites like (N-DABCO)$(NH_4)Br_3$ show the $\mu\tau$ product values in the 10^{-4} $cm^2\ V^{-1}$ range, with trap densities around 10^9 cm^{-3},[56] positioning them competitively with traditional semiconductor materials such as silicon and lead-based perovskite compositions (Table 1).[52,53]

In summary, the characteristics of MOPs stimulate their prospective applications for next-generation optoelectronic devices,[7] such as in sensing and photodetection. Their intrinsic characteristics are affected by external stimuli, such as temperature and pressure, determining structural, optoelectronic, and mechanical properties.

Mechanical properties

Unlike conventional metal–halide perovskites, stabilised by metal coordination, MOPs rely on hydrogen bonding networks. This makes them more susceptible to changes under external conditions, which directly impact their characteristics. In this regard, the absence of metal centres introduces structural flexibility that could lead to novel responses to stimuli, potentially altering performance in ferroelectric devices or sensors. Thus, understanding the effect of external stimuli is key to optimising their properties and applications.

Despite the absence of a metal-linker coordination bond, the mechanical strength of MOPs is comparable to that of hybrid organic–inorganic halide perovskites. For instance, (M-DABCO)NH_4I_3[11] and (PAZE)$NH_4Cl_3 \times 2H_2O$ exhibit bulk moduli of ~15 and 25 GPa,[32] respectively, which falls within the range of values typical for hybrid organic–inorganic perovskites, such as $CH_3NH_3PbI_3$ (14.8 GPa), $CH_3NH_3PbBr_3$ (17.6 GPa) and elpasolites such as $Cs_2AgInCl_6$ (23 GPa).[57] This suggests that the physical properties of (M-DABCO)NH_4I_3 are comparable to those of other perovskites, even though stabilised by hydrogen bonding interactions between $[NH_4]^+$ and I^- ions. This distinct molecular framework gives the material its characteristic properties, combining the structural stability of traditional perovskites with the versatility offered by organic components. Nanoindentation tests along the [111] orientation of the (M-DABCO)NH_4I_3 crystals yielded a Young's modulus of 14.7 GPa and a hardness of 0.78 GPa,[11,58] which is approximately 37% higher than that of $CH_3NH_3PbI_3$, suggesting good mechanical durability.[59] These properties make (M-DABCO)NH_4I_3 promising for thin-film ferroelectric devices, with potential applications in flexible electronics and devices with long-term stability and resistance to mechanical stress. Pressure-dependent Raman spectroscopy of (M-DABCO)NH_4I_3 revealed a progressive contraction of the unit cell from ambient until 10.2 GPa. At 12 GPa, the splitting of the Raman mode near 1090 cm^{-1} reveals the amorphisation-induced distortion of M-DABCO cations.[45] The pressure-dependent UV-vis absorption and PL measurements of the crystal under high pressure[45] revealed significant changes in optical properties. As the pressure increases to 14.5 GPa, two excitonic absorption peaks in the visible region progressively enhance, showing a piezochromic effect. The pressure-dependent band gap initially increases due to lattice distortion below 0.7 GPa, followed by a gradual decrease, as orbital coupling strengthens with further compression, leading to structural amorphisation above 10.4 GPa. PL measurements show that, under mild compression, the emission position remains stable below 0.7 GPa, with a blue shift occurring between 0.7 and 9.9 GPa due to lattice contraction. At higher pressures, up to 14.8 GPa, a red shift occurs, accompanied by distinct colour changes from orange to yellow to green, whereas (M-DABCO)NH_4I_3 exhibits emission enhancement in the 0.7–2.0 GPa and 4.5–8.9 GPa ranges.

Such structural dynamics are widely studied using temperature-dependent measurements, particularly during phase transitions, yet these investigations on MOPs remain limited.[60] Temperature-dependent powder X-ray diffraction measurements were performed on (M-DABCO)$NH_4(PF_6)_3$ and its deuterated counterpart, (MD-DABCO)$(NH_4)(PF_6)_3$, to track structural changes during phase transition. Upon increasing temperature, the diffraction peaks shift to lower angles, indicating an expansion of the unit cell. Additionally, the disappearance of certain peaks signals the transition from a ferroelectric to a more symmetric cubic cell in the paraelectric phase. Interestingly, these two phases coexist without intermediate states during the phase transition, suggesting a discontinuous, first-order order–disorder type transition. In addition, both compositions show an abrupt increase of dielectric permittivity around their phase transition temperature.[60] This opens interesting opportunities in the design of

mechanochromic and other stimuli-responsive materials and devices in the future.

Ferroelectric properties

The understanding of the optoelectronic and mechanical properties of MOPs remains somewhat limited, partly due to the challenges in fabricating thin films that are more compatible with spectroscopy techniques. However, their ferroelectric properties have been more extensively studied. These ferroelectric properties have drawn attention to this class of materials since they were first reported. For instance, (M-DABCO)NH_4I_3 showed high spontaneous polarisation intensity (P_s) close to conventional inorganic ferroelectrics as $BaTiO_3$ while featuring a higher phase-transition temperature (448 K *vs.* 393 K).[8] Similarly, hexamethylenetetramine-based (HMTA)NH_4Br_3 perovskites displayed ferroelectric behaviour up to 400 K, and ferroelectric polarisation was measured using single crystals and polycrystalline pellets.[61] Moreover, the functionalisation of the A site enabled large piezoelectric responses and multiaxial ferroelectric properties.[62,63] These reports reveal new perspectives for this material class.[7–10,12,32,33,41,47,60–63]

The origin of ferroelectric properties in MOPs has been rationalised by the combination of three critical factors, namely A-site polarity, preferred orientation (along ⟨111⟩ directions), and ferroelastic strain coupling, driving the ferroelectric transition.[2,3] Theoretical studies have also rationalised the absence of such polarisation in other halide perovskites, providing a set of design rules for perovskite ferroelectrics.[3] Initially, the use of polar A-site cations was considered critical since replacing M-DABCO (C_{3v} symmetry) with DABCO (D_{3h} point symmetry) led to the loss of the polar ground states for the ferroelectric transition.[8] This follows the "quasispherical theory," where the local polarisation arising from the asymmetric substitution of spherical A cations can be associated with the ferroelectric response. However, this was insufficient to describe other perovskites with polar A site cations (such as ($CH_3NH_3^+$)PbI_3), which are not polar.[9] To generate bulk polarisation, additional factors are required to couple the dipole orientations, such as the alignment along the ⟨111⟩ direction body diagonal of the perovskite cage that allows for hydrogen bonding between the A cations and halide anions around the common B cation, directing $[BX_3]^{2-}$ distortion (Fig. 4a).[3] This hydrogen bonding to the three anions makes them less available for other interactions, constraining the A cation orientation for long-range ferroelectric order, amplifying an effective dipole moment. Finally, the pairing of the through-space dipole interactions and strain coupling distortion—reflected in the tendency for the strains in the neighbouring cells to align---stabilises the polar ground state (*R*3 symmetry).[3] None of these interactions (*i.e.*, hydrogen bonding, dipolar interactions, and strain coupling) account for inversion-symmetry breaking individually (Fig. 4b). Instead, their combination enables polar ground states for ferroelectric transitions (Fig. 4c–e).[3] This sets the basis for more general material design rules beyond the DABCO perovskite family,[2,3] which should involve A site dipoles that orient preferentially along the ⟨111⟩ direction and feature ferroelastic strain coupling. Other mechanisms may emerge to describe the ferroelectric response and guide applications.

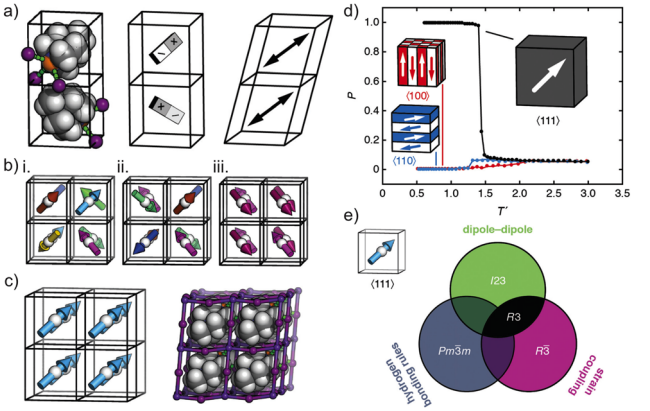

Fig. 4 Ferroelectric properties of MOPs. (a) Microscopic driving forces for the ferroelectric order: the tendency for each iodide (purple spheres) to hydrogen bonds with a single N–H proton (orange sphere; left), dipolar interactions (middle), and strain coupling (right). (b) Representative ground states for interactions in (a). Arrows denote the orientations of M-DABCO C_{3v} axes (*i.e.*, N–H bond vectors) and are coloured accordingly: (i) hydrogen-bonding interactions give a correlated-disordered ground state ($Pm\bar{3}m$ symmetry); (ii) dipolar interactions drive an ordered state (*I*23 symmetry); (iii) strain coupling gives a partially ordered (nematic) state (the average structure of $R\bar{3}$ symmetry). None of these states is polar. (c) A ferroelectric *R*3 phase with the corresponding DFT structure (right). The model satisfies the "hydrogen-bonding rule" that each iodide anion is strongly bonded to one M-DABCO. (d) Temperature dependence of the bulk polarisation using the Monte Carlo simulation. The traces correspond to the simulations in which local orientations are confined to ⟨111⟩ (black), ⟨110⟩ (blue), and ⟨100⟩ axes. The corresponding ground states are represented schematically; only ⟨111⟩ is polar. (e) Symmetry-breaking implications of the microscopic orientation-coupling mechanisms in MOPs. For perovskites with polar B-site cations aligned preferentially along ⟨111⟩ axes, the combinations of strain-coupling (pink) and dipole–dipole (green) interactions (black) are sufficient to stabilise the polar *R*3 ground state observed experimentally. Adapted from ref. 3 under CC-BY 3.0 licence. Copyright 2021 Royal Society of Chemistry.

Other properties and prospective applications

MOPs have already shown promise in various applications in the last few years, including sensing, X-ray detection, imaging, and field-effect transistors,[12,26,45,46,58] revealing new perspectives.

The structural flexibility and broad bandgap combined with stimuli-responsive and ferroelectric characteristics of MOPs open unique perspectives for sensing and detection applications. For instance, (H-DABCO)NH_4Br_3 crystals and their derivatives displayed great potential for X-ray detection due to their high $\mu\tau$ values, which indicate high sensitivity and low noise in detectors, aided by their low UV absorption coefficient. Moreover, compared to other lightweight sensors, like conjugated organic crystals, these MOPs offer higher X-ray attenuation and low operating voltage, making them ideal candidates for lightweight, high-energy radiation sensors and imaging.[12,45,46,58] They are also emerging as promising candidates for future field-effect transistors, thanks to their remarkable carrier diffusion lengths, low toxicity, and stability in air. Additionally, the

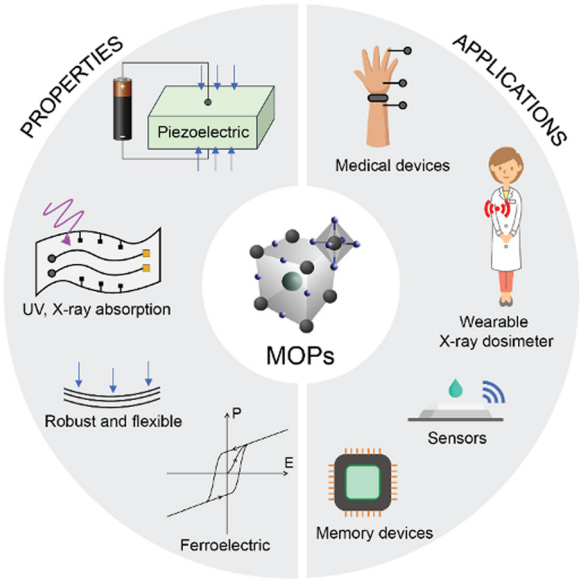

Fig. 5 Illustration showcasing the properties and prospective applications of MOPs. Relevant properties include piezoelectricity under mechanical stress, UV and X-ray absorption, robustness and flexibility, and ferroelectric behaviour. Applications range from wearable X-ray dosimeters and medical devices to advanced sensors and memory devices, highlighting the versatile potential of MOPs in various technological fields.

ease of growing single crystals to sizes of several centimetres hints at the potential for the production of large-scale integrated devices. Instead, the very large bandgap restricts their potential applications in photovoltaics, although their ferroelectric characteristics could improve photovoltaic performances through a bulk photoelectric effect.[64] However, their flexibility and light weight offer significant potential in flexible display applications. The main challenges and limitations lie in their need for further development in terms of compositional diversity and compatible processing conditions, while considering their hygroscopic character. Achieving desirable properties, such as colour tunability, broadband emission, and high PL quantum efficiencies with enhanced stability, remains crucial. These advancements are necessary for MOPs to become competitive in light, flexible, and wearable technologies (Fig. 5).

Summary and outlook

MOPs have emerged recently, offering environmentally friendly alternatives to conventional perovskite materials, which often contain toxic metal components. These materials exhibit promising ferroelectric properties and efficient charge transport, as well as mechanical strength, yet their development faces challenges, particularly related to their synthesis, stability, and integration into practical applications.

The synthesis approaches—ranging from solution-based single-crystal growth to mechanosynthesis—offer a balance between understanding intrinsic properties and scaling production for technological use. Single crystals remain essential for fundamental studies, providing insights into intrinsic optoelectronic, mechanical, and ferroelectric properties. However, the broader applicability of these materials lies in developing techniques that allow scalable production of high-quality polycrystalline powders and thin films, which can also facilitate further exploration of their optoelectronic properties. Mechanosynthesis has emerged as a particularly promising technique for producing perovskite materials on a larger scale, especially for compositions that present challenges in solution-based synthesis. It also allows for precise control over stoichiometry and particle sizes, as critical factors in optimising the material properties for specific device applications, such as thin-film transistors, photovoltaics, and light-emitting diodes. This level of control could contribute to improved material characteristics and device performance, which are crucial for large-scale integration and deployment. It would also permit expanding the material scope, such as toward low-dimensional[26] and electronically active materials,[10] as well as chiral perovskite analogues, among others. The method should offer more insights into structure–property relationships, enhance sustainability, and provide the potential to meet scalability, making it an attractive avenue for development.

The potential applications for MOPs are diverse despite the challenges posed by their synthetic accessibility. Their PL under UV excitation suggests that they could be well-suited for UV optoelectronics, including UV photodetectors, UV-emitting devices, and lasers. Additionally, their high bandgap makes them attractive candidates for use in transparent electronics, where minimal light absorption is required, as well as in protective coatings for devices exposed to high-energy radiation environments. Finally, the ferroelectric properties of these materials create opportunities for memory elements, whilst their strong ferroelectric behaviour at high temperatures and under environmentally benign conditions enhances their appeal for next-generation energy technologies. As research progresses in tuning the bandgap and improving charge transport properties, these materials may also find a broader use in flexible electronics and other emerging fields.

One of the primary challenges for applications of MOPs in LEDs and photovoltaics is their high energy bandgap. This limits their suitability for conventional optoelectronics, which require lower bandgaps (typically 1–2.5 eV) to efficiently absorb or emit light in the visible and near-infrared regions. If the bandgap can be tuned within the solar spectrum (*e.g.*, by substituting Br with I and possibly replacing the ammonium cation with other[1,7]), and the absorption coefficient is enhanced, these materials could offer a broader scope of applications.[10] Another obstacle in developing these materials is the limited availability of precursor materials, particularly A^{2+} cations, and their sensitivity to moisture and light.[48] Designing, synthesising, and functionalising these cations to tailor their properties requires extensive molecular engineering and computational screening, complemented with organic and material synthesis and characterisation, to ensure that they can achieve the desired bandgap and integrate effectively into the perovskite frameworks. Moreover, judicious molecular design can enhance their stability, while the use of mechanosynthesis

and fabrication of thin films can expand their scope and scalability. Although this is a resource-intensive process, advancements in molecular design and synthesis, complemented with theoretical investigations, could help unlock new compositions and bring MOPs in a broader range of future applications.

Author contributions

All authors contributed to the manuscript and discussion.

Data availability

This is a review article, and all the referred data and schematics have been previously published. The schematics and illustrations are available upon request.

Conflicts of interest

There are no conflicts to declare.

Acknowledgements

G. B. and J. V. M. are grateful to the Swiss National Science Foundation (SPARK project no. 221017) for financial support. The work of L. A. M. is part of the Dutch Research Council (NWO). J. V. M. appreciates the ERC Starting Grant (no. 101114653).

References

1 B. Saparov and D. B. Mitzi, *Chem. Rev.*, 2016, **116**, 4558–4596.
2 M. Manzi, G. Pica, M. De Bastiani, S. Kundu, G. Grancini and M. I. Saidaminov, *J. Phys. Chem. Lett.*, 2023, 3535–3552.
3 D. J. W. Allen, N. C. Bristowe, A. L. Goodwin and H. H.-M. Yeung, *J. Mater. Chem. C*, 2021, **9**, 2706–2711.
4 S. Horiuchi and Y. Tokura, *Nat. Mater. Rev.*, 2008, **7**, 357–367.
5 L. W. Martin and A. M. Rappe, *Nat. Rev. Mater.*, 2016, **2**, 1–14.
6 S. Shkuratov and C. Lynch, *J. Metriom.*, 2022, **8**, 739–752.
7 X. Song, G. Hodes, K. Zhao and S. F. Liu, *Adv. Energy Mater.*, 2021, **10**, 2003331.
8 H.-Y. Ye, Y.-Y. Tang, P.-F. Li, W.-Q. Liao, J.-X. Gao, X.-N. Hua, H. Cai, P.-P. Shi, Y.-M. You and R.-G. Xiong, *Science*, 2018, **361**, 151–155.
9 W.-Y. Zhang, Y.-Y. Tang, P.-F. Li, P.-P. Shi, W.-Q. Liao, D.-W. Fu, H.-Y. Ye, Y. Zhang and R.-G. Xiong, *J. Am. Chem. Soc.*, 2017, **139**, 10897–10902.
10 J. Bie, D.-B. Yang, M.-G. Ju, Q. Pan, Y.-M. You, W. Fa, X. C. Zeng and S. Chen, *JACS Au*, 2021, **1**, 475–483.
11 M. G. Ehrenreich, Z. Zeng, S. Burger, M. R. Warren, M. W. Gaultois, J.-C. Tan and G. Kieslich, *Chem. Commun.*, 2019, **55**, 3911–3914.
12 X. Song, Q. Cui, Y. Liu, Z. Xu, H. Cohen, C. Ma, Y. Fan, Y. Zhang, H. Ye, Z. Peng, R. Li, Y. Chen, J. Wang, H. Sun, Z. Yang, Z. Liu, Z. Yang, W. Huang, G. Hodes, S. (Frank) Liu and K. Zhao, *Adv. Mater.*, 2020, **32**, 2003353.
13 Q. Cui, N. Bu, X. Liu, H. Li, Z. Xu, X. Song, K. Zhao and S. F. Liu, *Nano Lett.*, 2022, **22**, 5973–5981.
14 T. S. Sherkar and L. Jan Anton Koster, *Phys. Chem. Chem. Phys.*, 2016, **18**, 331–338.
15 Y. Hou, C. Wu, D. Yang, T. Ye, V. G. Honavar, A. C. T. van Duin, K. Wang and S. Priya, *J. App. Phys.*, 2020, **128**, 060906.
16 I.-H. Park, Q. Zhang, K. C. Kwon, Z. Zhu, W. Yu, K. Leng, D. Giovanni, H. S. Choi, I. Abdelwahab, Q.-H. Xu, T. C. Sum and K. P. Loh, *J. Am. Chem. Soc.*, 2019, **141**, 15972–15976.
17 L. Li, X. Liu, C. He, S. Wang, C. Ji, X. Zhang, Z. Sun, S. Zhao, M. Hong and J. Luo, *J. Am. Chem. Soc.*, 2020, **142**, 1159–1163.
18 W. Zhang, M. Hong and J. Luo, *Angew. Chem., Int. Ed.*, 2020, **59**, 9305–9308.
19 P.-P. Shi, S.-Q. Lu, X.-J. Song, X.-G. Chen, W.-Q. Liao, P.-F. Li, Y.-Y. Tang and R.-G. Xiong, *J. Am. Chem. Soc.*, 2019, **141**, 18334–18340.
20 Y. Shang, Z.-H. Yu, R.-K. Huang, S.-L. Chen, D.-X. Liu, X.-X. Chen, W.-X. Zhang and X.-M. Chen, *Engineering*, 2020, **6**, 1013–1018.
21 C. A. Bremner, M. Simpson and W. T. A. Harrison, *J. Am. Chem. Soc.*, 2002, **124**, 10960–10961.
22 R. Pandey, G. Vats, J. Yun, C. R. Bowen, A. W. Y. Ho-Baillie, J. Seidel, K. T. Butler and S. I. Seok, *Adv. Mater.*, 2019, **6**, 1807376.
23 H.-Y. Liu, H.-Y. Zhang, X.-G. Chen and R.-G. Xiong, *J. Am. Chem. Soc.*, 2020, **142**, 15205–15218.
24 H.-Y. Zhang, Y.-Y. Tang, P.-P. Shi and R.-G. Xiong, *Acc. Chem. Res.*, 2019, **52**, 1928–1938.
25 P. Dong, C. Lin, N. Ye and M. Luo, *Angew. Chem., Int. Ed.*, 2024, **63**, e202407048.
26 H. S. Choi, J. Lin, G. Wang, W. P. D. Wong, I.-H. Park, F. Lin, J. Yin, K. Leng, J. Lin and K. P. Loh, *Science*, 2024, **384**, 60–66.
27 F. Cordero, F. Craciun, P. Imperatori, V. Raglione, G. Zanotti, A. Moldovan and M. Dinescu, *Materials*, 2023, **16**, 7323.
28 F. Lyu, Z. Chen, R. Shi, J. Yu and B.-L. Lin, *J. Solid State Chem.*, 2021, **304**, 122548.
29 F. Palazon, Y. El Ajjouri and H. J. Bolink, *Adv. Energy Mater.*, 2020, **10**, 1902499.
30 P. Ferdowsi, E. Ochoa-Martinez, U. Steiner and M. Saliba, *Chem. Mater.*, 2021, **33**, 3971–3979.
31 W. K. A. Al-Ithawi, A. F. Khasanov, I. S. Kovalev, I. L. Nikonov, V. A. Platonov, D. S. Kopchuk, S. Santra, G. V. Zyryanov and B. C. Ranu, *Polymers*, 2023, **15**, 1853.
32 K. Li, L.-Y. Dong, H.-X. Xu, Y. Qin, Z.-G. Li, M. Azeem, W. Li and X.-H. Bu, *Mater. Chem. Front.*, 2019, **3**, 1678–1685.
33 H. Wang, H. Liu, Z. Zhang, Z. Liu, Z. Lv, T. Li, W. Ju, H. Li, X. Cai and H. Han, *npj Comput. Mater.*, 2019, **5**, 17.
34 D. E. Crawford, C. K. G. Miskimmin, A. B. Albadarin, G. Walker and S. L. James, *Green Chem.*, 2017, **19**, 1507–1518.

35 G.-J. Lee, E.-K. Park, S.-A. Yang, J.-J. Park, S.-D. Bu and M.-K. Lee, *Sci. Rep.*, 2017, **7**, 46241.
36 S.-R. Bae, D. Y. Heo and S. Y. Kim, *Mater. Today Adv.*, 2022, **14**, 100232.
37 C. C. Li, T. Yu Huang, Y. H. Lai, Y. C. Huang and C. Shan Tan, *Mater. Today Electron.*, 2024, **8**, 100095.
38 N. Wang, L. Cheng, R. Ge, S. Zhang, Y. Miao, W. Zou, C. Yi, Y. Sun, Y. Cao, R. Yang, Y. Wei, Q. Guo, Y. Ke, M. Yu, Y. Jin, Y. Liu, Q. Ding, D. Di, L. Yang, G. Xing, H. Tian, C. Jin, F. Gao, R. H. Friend, J. Wang and W. Huang, *Nat. Photon.*, 2016, **10**, 699–704.
39 Z. Zhang, W. Chen, X. Jiang, J. Cao, H. Yang, H. Chen, F. Yang, Y. Shen, H. Yang, Q. Cheng, X. Chen, X. Tang, S. Kang, X. Ou, C. J. Brabec, Y. Li and Y. Li, *Nat. Energy*, 2024, **9**, 592–601.
40 Z. Ma, Z. Xiao, W. Zhou, L. Jin, D. Huang, H. Jiang, T. Yang, Y. Liu and Y. Huang, *J. Alloys Compd.*, 2020, **822**, 153539.
41 T. W. Kasel, Z. Deng, A. M. Mroz, C. H. Hendon, K. T. Butler and P. Canepa, *Chem. Sci.*, 2019, **10**, 8187–8194.
42 S. Meloni, G. Palermo, N. Ashari-Astani, M. Grätzel and U. Rothlisberger, *J. Mater. Chem. A*, 2016, **4**, 15997–16002.
43 K. T. Butler, J. M. Frost and A. Walsh, *Mater. Horiz.*, 2015, **2**, 228–231.
44 Z. Li, G. Peng, H. Chen, C. Shi, Z. Li and Z. Jin, *Angew. Chem., Int. Ed.*, 2022, **61**, e202207198.
45 X. Song, Q. Li, J. Han, C. Ma, Z. Xu, H. Li, P. Wang, Z. Yang, Q. Cui, L. Gao, Z. Quan, S. (Frank) Liu and K. Zhao, *Adv. Mater.*, 2021, **33**, 2102190.
46 Z. Li, Z. Li, G. Peng, C. Shi, H. Wang, S.-Y. Ding, Q. Wang, Z. Liu and Z. Jin, *Adv. Mater.*, 2023, **35**, 2300480.
47 T. Handa, R. Hashimoto, G. Yumoto, T. Nakamura, A. Wakamiya and Y. Kanemitsu, *Sci. Adv.*, 2022, **8**, eabo1621.
48 J. Zhang, H. Ma, X. Zhang and Y. Ma, *J. Phys. Chem. Lett.*, 2022, **13**, 9848–9854.
49 S. J. Zelewski, J. M. Urban, A. Surrente, D. K. Maude, A. Kuc, L. Schade, R. D. Johnson, M. Dollmann, P. K. Nayak, H. J. Snaith, P. Radaelli, R. Kudrawiec, R. J. Nicholas, P. Plochocka and M. Baranowski, *J. Mater. Chem. C*, 2019, **7**, 8350–8356.
50 J.-H. Wei, J.-F. Liao, X.-D. Wang, L. Zhou, Y. Jiang and D.-B. Kuang, *Matter*, 2020, **3**, 892–903.
51 L. Zhou, J.-F. Liao, Z.-G. Huang, J.-H. Wei, X.-D. Wang, W.-G. Li, H.-Y. Chen, D.-B. Kuang and C.-Y. Su, *Angew. Chem., Int. Ed.*, 2019, **58**, 5277–5281.
52 H. Mescher, F. Schackmar, H. Eggers, T. Abzieher, M. Zuber, E. Hamann, T. Baumbach, B. S. Richards, G. Hernandez-Sosa, U. W. Paetzold and U. Lemmer, *ACS Appl. Mater. Interfaces*, 2020, **12**, 15774–15784.
53 S. O. Kasap, *J. Phys. D: Appl. Phys.*, 2000, **33**, 2853–2865.
54 J. R. Ayres, *J. App. Phys.*, 1993, **74**, 1787–1792.
55 A. Balcioglu, R. K. Ahrenkiel and F. Hasoon, *J. App. Phys.*, 2000, **88**, 7175–7178.
56 Z. Li, Y. Pang, G. Peng, H. Wang, Q. Li, X. Zhou, Z. Li, Q. Wang and Z. Jin, *J. Phys. Chem. Lett.*, 2024, **15**, 4375–4383.
57 L. A. Muscarella, H. J. Jöbsis, B. Baumgartner, P. T. Prins, D. N. Maaskant, A. V. Petukhov, D. Chernyshov, C. J. McMonagle and E. M. Hutter, *J. Phys. Chem. Lett.*, 2023, **14**, 9042–9051.
58 Q. Cui, X. Song, Y. Liu, Z. Xu, H. Ye, Z. Yang, K. Zhao and S. (Frank) Liu, *Matter*, 2021, **4**, 2490–2507.
59 Y. Rakita, S. R. Cohen, N. K. Kedem, G. Hodes and D. Cahen, *MRS Commun.*, 2015, **5**, 623–629.
60 H. S. Choi, S. Li, I.-H. Park, W. H. Liew, Z. Zhu, K. C. Kwon, L. Wang, I.-H. Oh, S. Zheng, C. Su, Q.-H. Xu, K. Yao, F. Pan and K. P. Loh, *Nat. Commun.*, 2022, **13**, 794.
61 H. Morita, R. Tsunashima, S. Nishihara, K. Inoue, Y. Omura, Y. Suzuki, J. Kawamata, N. Hoshino and T. Akutagawa, *Angew. Chem., Int. Ed.*, 2019, **58**, 9184–9187.
62 H. Zhang, Z.-K. Xu, Z.-X. Wang, H. Yu, H.-P. Lv, P.-F. Li, W.-Q. Liao and R.-G. Xiong, *J. Am. Chem. Soc.*, 2023, **145**, 4892–4899.
63 Z.-X. Zhang, H.-F. Ni, J.-S. Tang, P.-Z. Huang, J.-Q. Luo, F.-W. Zhang, J.-H. Lin, Q.-Q. Jia, G. Teri, C.-F. Wang, D.-W. Fu and Y. Zhang, *J. Am. Chem. Soc.*, 2024, **146**, 27443–27450.
64 Z. Dai and A. M. Rappe, *Chem. Phys. Rev.*, 2023, **4**, 011303.

